

Response to Editor:

Thank you for submitting your manuscript entitled "Intensified Atlantic vs. weakened Pacific meridional overturning circulations in response to Tibetan Plateau uplift" [Paper #cp-2017-110] to *Climate of the Past*. I have now received an assessment of the two reviewers. Both reviewers had positive comments that require a minor revision prior to the publication of *Climate of the Past*.

Following reviewers concerns shall be addressed in the revised version to improve the quality of the manuscript:

1) Why does a removal of Tibetan Plateau leads to the intensified westerlies over the North Atlantic and weakened subtropical anticyclones and trade winds over the Pacific? Are these changes a direct atmospheric response of TP removal, or including feedbacks of SST?

In the last version of the manuscript (version-20180321-mark), we had addressed this issue accordingly, and at that time we had also replied as follows in our reply-to-reviewer file.

First, the intensified westerlies over the North Atlantic in response to the TP removal is due to the absence of barrier effect from the TP allowing the atmospheric jet stream and associated low-level winds to become more zonal. Besides, the standing waves in association with the TP removal are also absent, leading to less orographic gravity wave drag and stronger winds (Palmer et al., 1986; Sinha et al., 2012). As shown in the revised version, the intensified surface westerly winds over the upstream of TP are clearly simulated (Fig. 2c on page 22).

Meanwhile, both theoretical studies and numerical simulations have demonstrated that the TP uplift strengthens the Asian summer monsoon and in turn diabatic heating over the Asian monsoon region, which provides a critical role in the formation and

maintenance of the summer North Pacific subtropical high (Ruddiman and Kutzbach, 1989; Rodwell and Hoskins, 2001; Kitoh, 2004). In particular, during the summertime, the upper-level divergence associated with strong monsoonal ascending motion is located over the Asian region and adjacent oceans, while the upper level convergence circulation related to the descending motion is observed over the middle and lower latitudes of eastern Pacific (Please see the following Fig. S1a). Comparatively, this circulation cell in the NTP is not as strong as in the MTP, indicating the weakening of both the North Pacific subtropical high and Asian monsoon (Please see the following Figs. S1b and S1c).

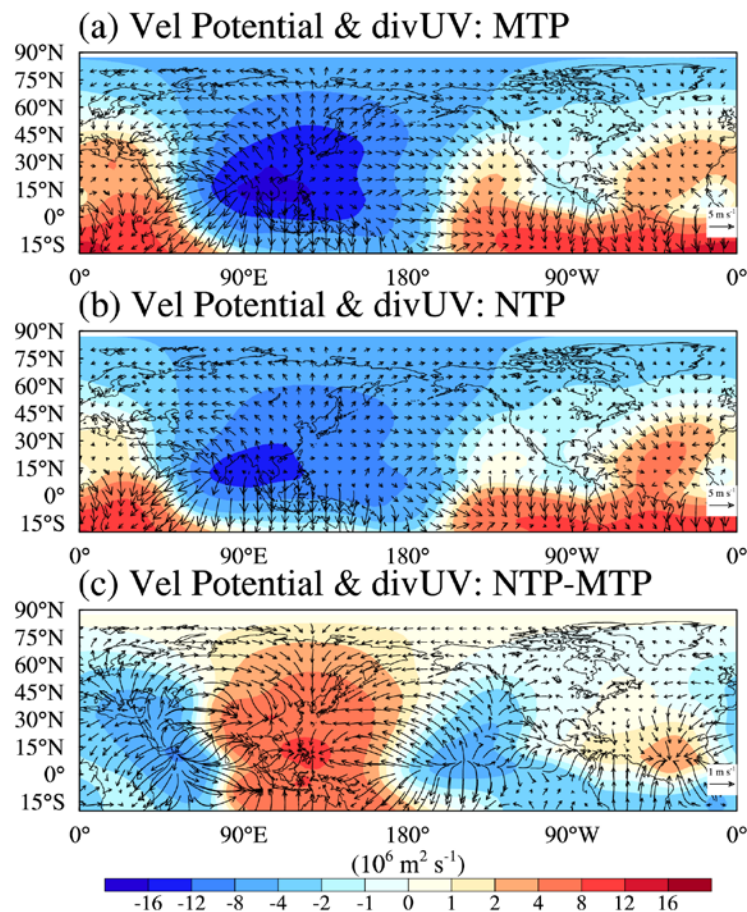


Figure S1. The Northern Hemisphere summertime mean velocity potential (contour) and divergent wind (vectors) at 200 hPa for the (a) MTP, (b) NTP, and (c) the differences between NTP and MTP.

Second, following your comment, we have supplemented a set of experiments with and without TP undertaken by the atmospheric general circulation model (AGCM) of CESM version 1.0.5, aiming to examine the feedback originating from the sea surface temperature changes. The 200-year climatologically averaged sea surface temperature prescribed in both the AGCM experiments is obtained from the MTP experiments undertaken by coupled atmosphere–ocean general circulation model (CGCM, CESM version 1.0.5). Both AGCM experiments are integrated for 50 model years, and the further analysis is performed based on the results of the last 30-year simulations.

In the CGCM experiments, the removal of the TP significantly causes a weakening of the North Pacific subtropical high and an overall weakening of the low-level tropical trade winds (Please see the following Fig. S2a). Similar changes are seen in the AGCM experiments, but with an overall weaker intensity (Please see the following Fig. S2b). Relative to the results of AGCM experiments, there is a clear decrease of tropical trade winds over the North Pacific and an increase of low-level westerly over the North Atlantic in the CGCM experiments (Please see the following Fig. S2c), indicating that the changes of sea surface temperature and oceanic circulations further amplify atmospheric circulation anomalies due to the TP uplift. Thus, we believe that the decrease of AMOC in our simulations is primarily attributed to the direct response of atmospheric circulation to the removal of the TP, and the oceanic feedback further amplifies this response. Considering the aforementioned atmospheric responses in association with the TP uplift have been addressed by many AGCM and CGCM simulations, we do not describe them in detail. Alternatively, we have added a short description on these processes in the revised version (L149–154).

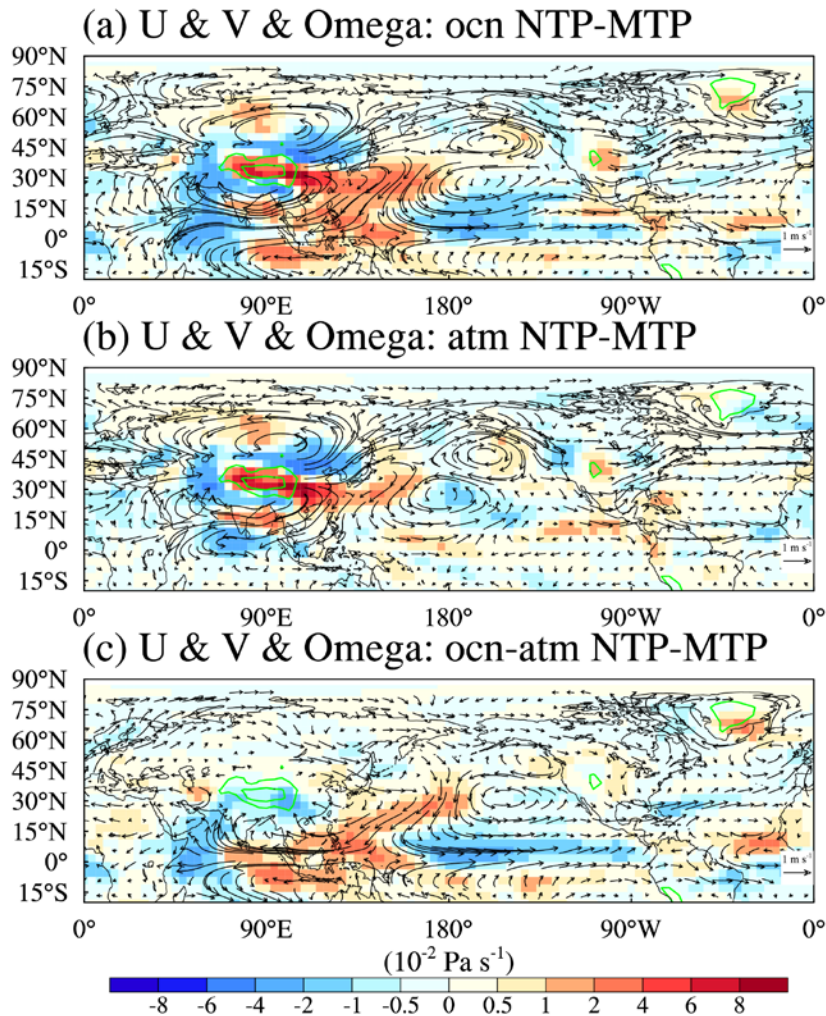


Figure S2. Changes of annual mean 500 hPa vertical velocity and 850 hPa wind in NTP relative to MTP for the (a) CGCM, (b) AGCM, and (c) differences between CGCM and AGCM. Green contours surround the areas with topography higher than 2000 m and 4000 m, respectively.

For details, please refer to L149–156 in the current version of the manuscript.

2) In the NTP experiment, the net freshwater flux increases by 0.005 Sv at the initial stage, but by 0.025 Sv at the final stage. The author should discuss if fresh water flux of 0.005Sv is strong enough to trigger the weakening of AMOC.

In the last version of the manuscript (version-20180321-mark), we had addressed this issue accordingly, and at that time we had also replied as follows in our reply-to-reviewer file.

We have compared the magnitude of net freshwater flux in our simulations with two earlier simulations, although there exists difference in the experimental configuration. Sinha et al. (2012) indicated a final net precipitation flux anomaly of approximately 0.02 Sv across the Atlantic basin (30–60°N). Maffre et al. (2017) indicated that the net freshwater flux anomaly over the North Atlantic (22–60°N) is approximately 0.0446 Sv and 0.097 Sv at the beginning and final stages, respectively. First, it should be noted that these two previous simulations with respect to the freshwater flux anomaly are obtained from simulations with and without global mountains, rather than the TP alone in our experiments. As such, the atmospheric circulation responses to the topographic modification in their experiments might be stronger than ours. Second, the area that they calculated the freshwater flux is over the North Atlantic at 22–60°N, and the grid mesh is greater in size than ours at 40–70°N. Third, Maffre et al. (2017) emphasized the net freshwater flux over the tropical Atlantic could play an important role in the AMOC weakening. We do not exclude the importance of the net freshwater flux over the tropical–subtropical Atlantic, since it has been well revealed that the warm and salty waters of the tropical–subtropical North Atlantic circulate north to the sub-polar regions of the North Atlantic via the Gulf Stream, and evaporation causes the surface waters to cool and thus the formation of North Atlantic Deep Water. Even though the net freshwater flux in our simulations is less than that in Maffre et al. (2017), it is difficult for us to determine the sensitivity of AMOC in response to the net freshwater flux in our simulations. Because we have identified the important role of wind-driven sea-ice process in initially triggering the AMOC weakening in our simulations. Thus, to answer the abovementioned question, a series of sensitivity experiments with the modification of

the net freshwater flux are necessary to be performed. However, this topic is beyond the scope of this study and needs to be investigated in the future.

Furthermore, we have added a preliminary comparison with recent simulations with and without global mountains in the current version (L169–174): “It should be noted that these changes in freshwater budget in our simulations are less than approximately 0.0446 Sv and 0.097 Sv of recent simulations with and without global mountains (Maffre et al., 2017), and the time for a complete collapse the AMOC in our NTP simulation (Figure 3b) is also longer (approximately 700 years) than for their experiments without global mountains (approximately 400 years). Such a difference should be related to the experimental design and the sensitivity of the models to freshwater forcing.”.

3) The T31 version of CESM is known to have significant climate biases, especially in high-latitude regions that are a main focus for this paper (including Arctic sea ice extent). Implications of these model biases on the results and conclusions shall be discussed.

In the last version of the manuscript (version-20180321-mark), we had addressed this issue accordingly, and at that time we had also replied as follows in our reply-to-reviewer file.

We agree that the low resolution version of CESM has a cold bias against the observation, especially in the North Atlantic high latitudes, which is partly attributed to the deficit of ocean heat transport and the excess of Arctic sea-ice (Shields et al., 2012). More specifically, in the pre-industrial simulation (MTP), there is a weak positive slope in the long-term global mean temperature, in particular at the beginning of simulations; and global mean temperature reaches a quasi-equilibrium state at approximately 12 °C,

which is lower than observations (please see Fig. 1c on page 21). In the revised version, we have mentioned this model bias and its potential influence on the simulations (L257–259).

For details on the model bias and its implications, please refer to L263–266 in the current version of the manuscript.

4) Avoid use of "vs." in the title and replace it with the word "difference" e.g. "Difference between the Atlantic and Pacific meridional overturning circulation in response to the uplift of the Tibetan Plateau"

The suggested title has been taken in the revised version. Thanks a lot!

The current marked-up manuscript version relative to the version-20180321:

1 ~~**Intensified Atlantic vs. weakened Pacific meridional overturning**~~
2 ~~**circulations in response to Tibetan Plateau uplift**~~ **Difference between**
3 **the North Atlantic and Pacific meridional overturning circulation in**
4 **response to the uplift of the Tibetan Plateau**

5 Baohuang Su^{1,4}, Dabang Jiang^{1,2,3,4}, Ran Zhang¹, Pierre Sepulchre⁵, and Gilles Ramstein⁵

6 ¹Institute of Atmospheric Physics, Chinese Academy of Sciences, Beijing 100029, China

7 ²Joint Laboratory for Climate and Environmental Change at Chengdu University of Information Technology,
8 Chengdu 610225, China

9 ³CAS Center for Excellence in Tibetan Plateau Earth Sciences, Beijing 100101, China

10 ⁴University of Chinese Academy of Sciences, Beijing 100049, China

11 ⁵Laboratoire des Sciences du Climat et de l'Environnement/IPSL, CEA-CNRS-UVSQ, UMR8212, Orme des
12 Merisiers, CE Saclay, 91191 Gif-sur-Yvette Cedex, France

13 **Abstract:** The role of the Tibetan Plateau (TP) in maintaining the large-scale overturning
14 circulation in the Atlantic and Pacific is investigated using a coupled atmosphere–ocean model. For
15 the present day with a realistic topography, model simulation shows a strong Atlantic meridional
16 overturning circulation (AMOC) but a near absence of the Pacific meridional overturning
17 circulation (PMOC), which are in good agreement with the present observations. In contrast, the
18 simulation without the TP depicts a collapsed AMOC and a strong PMOC that dominates deep
19 water formation. The switch in deep water formation between the two basins results from changes
20 in the large-scale atmospheric circulation and atmosphere–ocean feedback over the Atlantic and
21 Pacific. The intensified westerly winds and increased freshwater flux over the North Atlantic cause
22 an initial slowdown of the AMOC, while the weakened East Asian monsoon circulation and
23 associated decreased freshwater flux over the North Pacific give rise to the initial intensification of

24 the PMOC. The further decreased heat flux and the associated increase in sea-ice fraction promote
25 the final AMOC collapse over the Atlantic, while the further increased heat flux leads to the final
26 PMOC establishment over the Pacific. Although the simulations were done in a cold world, it still
27 importantly implicates that the uplift of the TP alone could have been a potential driver for the
28 reorganization of PMOC–AMOC between the Late Eocene and Early Oligocene.

29 1. Introduction

30 The uplift of the Tibetan Plateau (TP) was a major tectonic event that had occurred throughout
31 the Cenozoic, and its gradual growth had exerted a strong influence on the atmospheric circulation
32 and climate (Molnar et al., 2010). Since the pioneering work of Bolin (1950), the impacts of
33 mountain uplift on regional and global climate have been extensively investigated. Nevertheless,
34 most studies have emphasized the role of mountain ranges on atmosphere dynamics, while
35 quantifications of the associated impact on ocean dynamics have been rare. For example, most
36 previous works have taken atmospheric general circulation models to address regional climate
37 effects, notably the Asian monsoon and arid environment evolutions (e.g., Ruddiman and Kutzbach,
38 1989; Ramstein et al., 1997; An et al., 2001; Liu and Yin, 2002; Jiang et al., 2008; Zhang et al.,
39 2015). However, simulations have recently been applied to investigate the effect of mountain uplift
40 in the context of the atmosphere–ocean system, and a few studies have proposed that the uplift of
41 the Andes (Sepulchre et al., 2009) and Rocky Mountains (Seager et al., 2002) is closely linked to
42 the evolution of oceanic circulations, including the Gulf Stream and Humboldt Current, and the El
43 Niño–Southern Oscillation system (Feng and Poulsen, 2014). Although it has been indicated that
44 the TP uplift affects sea surface temperatures, sea surface salinity, precipitation, and trade winds for
45 both the Pacific and equatorial Indian Ocean (Abe et al., 2003; Kitoh, 2004; Okajima and Xie,
46 2007), the influence of the TP uplift on the high-latitude oceanic circulations, particularly in the
47 North Atlantic, has rarely been explored.

48 The potential importance of mountain uplift in modifying the oceanic thermohaline circulation

49 has previously been investigated. Ruddiman and Kutzbach (1989) indicated that mountain
50 uplift-induced changes in the North Atlantic surface circulation are expected to increase the North
51 Atlantic Deep Water formation. In addition, Rind et al. (1997) performed the coupled model
52 simulations with and without TP and proposed that the TP may have a considerable impact on the
53 large-scale meridional overturning circulation (MOC). However, the integration time used in this
54 pioneering simulations was too short to fully evaluate the deep oceanic circulation response, and
55 thus more studies are still needed to evaluate the possible role of the TP in modulating the MOC.

56 On a geological timescale, remarkable reorganization and evolution of the large-scale oceanic
57 overturning circulation, from the Southern Ocean deep water dominating mode to the modern-like
58 North Atlantic deep water mode, have been evidenced through the Late Eocene to the Early
59 Oligocene (Wright and Miller, 1993; Davies et al., 2001; Via and Thomas, 2006). This dramatic
60 shift is possibly associated with major rearrangements in the ocean seaways and other tectonic
61 changes, although the ultimate trigger is still being debated (Zhang et al., 2011). In addition, it is
62 suggested that the regional surface of the TP had reached a high elevation of more than 4000 meters
63 around 40 Ma ago (Dupont-Nivet et al., 2008; Wang et al., 2008), although debates regarding
64 paleoaltitude reconstructions remain (Botsyun et al., 2016). Given this timing of TP uplift, it is
65 important to quantify the contribution of TP uplift on the meridional oceanic circulation of the
66 Northern Hemisphere. In this study, therefore, two coupled atmosphere–ocean numerical
67 integrations, with and without TP, are designed to investigate the role of the TP on the Atlantic
68 MOC (AMOC) and Pacific MOC (PMOC).

69 2. Model, experimental design, and density flux analysis

70 2.1. Model and experiments

71 The Community Earth System Model (CESM) version 1.0.5 of the National Center for
72 Atmospheric Research is a widely used, well-validated coupled model with dynamic atmosphere,
73 land, ocean, and sea-ice components (Gent et al., 2011). It is applied to this study at a

74 low-resolution configuration that is computationally efficient and well-described (Shields et al.,
75 2012) and employs an atmospheric horizontal grid of roughly $3.75^\circ \times 3.75^\circ$ (T31) with 26 vertical
76 levels. The ocean model adopts a finer oceanic horizontal grid, with a nominal 3° resolution
77 increasing to 1° near the equator (116×100 grid points, latitude by longitude) and 60 unevenly
78 spaced layers in the vertical direction. The sea-ice and land models share the same horizontal grids
79 as the ocean and atmosphere models, respectively, where the sea-ice component is a
80 dynamic–thermodynamic model that includes a subgrid-scale ice thickness distribution and
81 energy-conserving thermodynamics (Holland et al., 2012).

82 Two experiments are conducted; firstly, a control run with the modern topography (MTP,
83 Figure 1a), and secondly a sensitivity run where topography within the region of $20\text{--}60^\circ\text{N}$ and
84 $60\text{--}140^\circ\text{E}$ at altitudes higher than 200 m is set to 200 m (NTP, Figure 1b), which enables
85 examination of the climate effect in relation to the TP topography. This TP uplift configuration has
86 been referred to in the majority of previous simulation works (e.g., Liu and Yin, 2002; Jiang et al.,
87 2008). This greatly simplified topographic setting is not intended to represent a realistic scenario
88 constrained by the geological evidence and instead represents two end-members of the potential
89 growth histories of the TP. So, it is important to note that these experiments only aim to investigate
90 the TP uplift occurring in “a cold world” with an atmospheric CO_2 corresponding to the
91 pre-industrial values (284.0 ppm). With the exception of topography, all the other boundaries, such
92 as land–sea distribution and orbital parameters, are prescribed to pre-industrial conditions. The MTP
93 is continually integrated for 1100 years, and the NTP is additionally integrated for another 1840
94 years starting from the year 1100 of the MTP. Global mean surface air temperature and sea
95 temperature at a depth of 1000 m are shown in Figure 1c. Both simulations reach equilibrium states
96 after more than 1000 model years of integration time, and the final 200 years of both cases are
97 applied for our climate state analysis.

98 2.2. Density flux analysis

99 Because one of the major aims of this paper is to analyze changes in the meridional oceanic
 100 circulation, we decided to focus on the density flux parameter, which is appropriate to diagnose
 101 these oceanic circulation changes. The dense deep water masses are formed in the area with
 102 relatively high surface density achieved by cooling or increasing salinity. To better understand
 103 which processes dominated the MOC changes in simulations, it is instructive to further analyze the
 104 time evolution of density fluxes budget. Therefore, a density flux analysis method, in which the
 105 total density flux decomposes into the haline contribution due to freshwater flux and the thermal
 106 contribution due to heat flux (Schmitt et al., 1989), is adopted in our study. The total density flux is
 107 calculated from a linearized state equation of seawater, as

$$F_{\rho} = -\alpha \cdot \frac{Q}{C_p} + \rho(0, T) \cdot \beta \cdot \frac{(E - P - R - I) \cdot S}{1 - S}$$

108 F_{ρ} is the total density flux, $-\alpha \cdot \frac{Q}{C_p}$ is thermal density flux, and $\rho(0, T) \cdot \beta \cdot \frac{(E - P - R - I) \cdot S}{1 - S}$ is haline
 109 density term. C_p , T , and S are the specific heat capacity, surface temperature and salinity of
 110 seawater, respectively. α and β are the thermal expansion and haline contraction coefficients,
 111 respectively. $\rho(0, T)$ is the density of freshwater with a salinity of 0 psu and temperature of T . Q
 112 represents the net surface heat flux. E , P , R , and I denote the freshwater fluxes due to
 113 evaporation, precipitation, river runoff, and sea-ice melting (or brine rejection), respectively.

114 3. Results

115 3.1. Changes in AMOC and PMOC

116 There are evident changes in the AMOC and PMOC indices in response to the TP uplift
 117 (Figure 1d). With MTP, the AMOC stabilizes at around 17 Sv ($\text{Sv} = 10^6 \text{ m}^3 \text{ s}^{-1}$) for more than 1000
 118 years (Figure 1d, 1–1100 years, red line), which agrees with the observations 18.7 ± 5.6 Sv for
 119 2004–2005 (Cunningham et al., 2007), but with NTP there is a continual weakening of the AMOC
 120 until the point of quasi-collapse (ca. 2 Sv, Figure 1d). In contrast, the PMOC of NTP begins at a
 121 sluggish level from MTP (Figure 1d, 1–1100 years, purple line) and takes as long as 1200 years to

122 reach an equilibrium state that is comparable to the level of the AMOC in MTP (ca. 18 Sv, Figure
123 1d, 1101–2940 years, purple line). In agreement with the dramatic responses of AMOC and PMOC,
124 sea surface salinity increases in the North Pacific but decreases in a broad area of the North Atlantic
125 (Figure 2b). To fully understand the different behaviors between AMOC and PMOC in NTP, in the
126 following sections we further analyze changes in the atmospheric and oceanic circulations and the
127 atmosphere–ocean feedbacks.

128 3.2. Atmospheric responses

129 The modified AMOC and PMOC are linked to the large-scale atmospheric circulation changes.
130 In terms of model results of the NTP relative to the MTP, the surface air temperature over and
131 around the TP and in the North Pacific increased but decreased over the North Atlantic (Figure 2a),
132 which agrees with the previous simulations (Broccoli and Manabe, 1992; Kutzbach et al., 1993). In
133 addition, there are intensified westerlies over the North Atlantic and weakened subtropical
134 anticyclones and trade winds over the North Pacific (Figure 2c); the former results from a
135 significant increase in the meridional pressure gradient driven by a large-scale equatorward shift of
136 air mass occupying the current position of the TP (Figure 2c) and from a reduced drag of the
137 orographically induced gravity waves associated with the absence of the TP (Palmer et al., 1986;
138 Sinha et al., 2012), while the latter is derived from the weakening of zonal Eurasia–Pacific thermal
139 contrast in the middle troposphere (not shown), especially in boreal summertime, in relation to
140 removal of the mountains (Ruddiman and Kutzbach, 1989; Rodwell and Hoskins, 2001; Kitoh,
141 2004).

142 When the TP is removed, the atmospheric moisture transport between the Pacific and Atlantic
143 Oceans undergoes a basin-basin asymmetric redistribution as a response to the large-scale
144 circulation anomalies (Figure 2c). In comparison with MTP results, the NTP simulation shows large
145 amounts of anomalous westerly moisture flux transported through the lowlands of Central America
146 to the North Atlantic, causing weak moisture convergence therein (Figure 2d). In addition, removal

147 of the TP leads to a significant divergence of moisture over East Asia and the western North Pacific
148 marginal seas (Figure 2d), which is linked to a weakened monsoon circulation and is consistent with
149 the previous simulations using both atmospheric and coupled ocean–atmosphere general circulation
150 models (Liu and Yin, 2002; Kitoh, 2004; Molnar et al., 2010). The anomalies of atmospheric
151 circulation shown above are derived partially from the positive feedback caused by the changed sea
152 surface temperature due to the removal of the TP. In particular, the weakening of both the Asian
153 monsoon and North Pacific subtropical anticyclone in association with the TP removal ~~were~~are
154 shown to be greater in the context of coupled model as compared to that in atmosphere-only model
155 due to the additional ocean–atmosphere feedback (Kitoh, 2004). Thus, the atmosphere–ocean
156 feedbacks also play an important role in maintaining the inter-basin atmospheric moisture
157 asymmetric redistribution.

158 3.3. Oceanic responses and atmosphere–ocean feedbacks

159 3.3.1. Changes in freshwater and sea-ice

160 The above changes in the large-scale atmospheric circulation markedly decrease the total
161 ocean density flux in the North Atlantic (Figure 3a, brown), supporting the trend of the AMOC
162 (Figure 1d). Both the increases of net freshwater and wind-driven sea-ice expansion are responsible
163 for the initial reduction of total ocean density flux and further induce a gradual weakening of the
164 AMOC. In more details, on the one hand, the anomalous atmospheric circulation associated with
165 the removal of the TP ~~transports~~drives more water vapor ~~transportation~~ northward (Figure 2d)
166 over the North Atlantic Ocean, causing more precipitation at the beginning of NTP simulation
167 (Figure 3b, ca. 1101–1200 years, red line). Correspondingly, the net freshwater flux (precipitation
168 plus runoff minus evaporation) convergence into the North Atlantic basin at 40°–70°N increases by
169 0.005 Sv (~3%) and 0.025 Sv (~16%) at the initial and final states of NTP simulations (Figure 3b,
170 green), respectively. It should be noted that these changes in freshwater budget in our simulations
171 are less than approximately 0.0446 Sv and 0.097 Sv of recent simulations with and without global

172 mountains (Maffre et al., 2017), and the time for a complete collapse of the AMOC in our NTP
173 simulation (Figure 3b) is also longer (approximately 700 years) than for their experiments without
174 global mountains (approximately 400 years). Such a difference should be related to the
175 experimental design and the sensitivity of the models to freshwater forcing.

176 ~~Moreover,~~ There is also a significant increase in the area-averaged sea-ice coverage over the
177 North Atlantic through wind-driven processes (Figure 3c, green). With the TP, the annual mean
178 sea-ice forms mainly in the northern and western region of the sub-polar North Atlantic, and it shifts
179 southward and eastward when driven by cyclonic wind stress associated with the Icelandic Low,
180 and melts in the Labrador Sea (sub-polar gyre) caused by a warm condition (Figure 4a). By
181 comparison, after removal of the TP, anomalously intensified cyclonic winds induce an anomalous
182 eastward sea-ice velocity (Figure 4c), and ~~cause~~ also a rapid eastward shift of the sea-ice margin
183 (Figure 4c). Meanwhile, the locally melted sea-ice due to thermodynamics processes reduces in the
184 southeast of Greenland (red shading, Fig. 4c), but increases in the south of Greenland (blue shading,
185 Fig. 4c). It suggests that there is more sea-ice transporting from the high latitudes into the sub-polar
186 gyre region, and the anomalous expansion of sea-ice margin in this region primarily originates from
187 the wind-driven eastward transportation (dynamics processes), but not the local formation
188 (thermodynamic processes). Because of this increased sea-ice through thermodynamically
189 insulating the sea water from the freezing air, the release of sensible and latent heat into the
190 atmosphere decreases and the density of sea water finally reduces, which processes have also been
191 previously elucidated by Zhu et al. (2014).

192 Moreover, the total ocean density flux increases in the North Pacific in response to the removal
193 of the TP. Due to the weakened Asian monsoon circulation and associated decrease in rainfall and
194 runoff after lowering the topography, the net freshwater flux received by the North Pacific decreases
195 by 0.08 Sv (~26%) and 0.12 Sv (~40%) during the initial and end stages of the NTP simulation,
196 respectively (Figure 6b, green). This continuous negative freshwater flux forcing tends to increase
197 density and initially leads to the formation of the North Pacific dense water, which is verified from

198 changes in the haline density flux (Figure 6a). Specifically, during the first 200 years of the NTP run,
199 the haline density flux constantly produces a net positive contribution to the total density relative to
200 the MTP haline term (Figure 6a, blue line). Meanwhile, the thermal density flux remains at a lower
201 level (Figure 6a, ca. 1101–1300 years, red line) relative to the MTP. Thus, it indicates that the
202 initially increased density of the North Pacific is largely attributed to the haline density term, but
203 not the thermal density term.

204 3.3.2. Roles of the atmosphere–ocean feedbacks

205 The aforementioned weakening of the AMOC due to the atmospheric processes further triggers
206 a positive atmosphere–ocean feedback loop through reducing northward heat transport, and
207 subsequent decreasing sea surface temperatures, then allowing sea-ice to expand, suppressing the
208 release of evaporating latent and sensible heat, and reducing the sea water density, and further
209 weakening the AMOC, as previously shown in Jayne and Marotzke (1999) and Zhu et al. (2014).

210 Note that the negative effect of net freshwater becomes increasingly unimportant in
211 comparison~~compared~~ to the heat flux feedback associated with the latent/sensible heat changes
212 (Figure 3a). Finally, the thermal density flux decreases by 49% relative to the MTP run, which
213 substantially dominates the total density flux changes (Figure 3a). To be specific, the annual mean
214 total density flux and mixed layer depth over the North Atlantic, especially around the Iceland
215 where the collapse of deep water formation occurs, is dramatically decreased in NTP (Figure 5d, the
216 maximum mixed layer depth is approximately 100 m) in comparison to that in MTP (Figure 5a, the
217 maximum mixed layer depth is approximately 900 m). Moreover, this reduced total density flux
218 over the North Atlantic is more attributed to the decreased thermal density flux associated with less
219 latent and sensible release (Figure 5e) than the changed haline density flux (Figure 5f).

220 Atmosphere–ocean feedbacks also strengthen the PMOC. Due to the initial development of the
221 PMOC mentioned in section 3.1, a positive feedback (as pointed out in Warren (1983)) is initiated
222 by the intensifying meridional oceanic circulation; which this transports warmer subtropical water

223 northward and leads to the buoyancy loss and evaporation increase (Figure 6b). This feedback is
224 also able to re-trigger PMOC enhancement. By comparison to the changes in the North Atlantic,
225 both the regionally averaged sea-ice coverage (Figure 6c) and February sea-ice margin (Figure 4f)
226 over the North Pacific experience a slightly northward retreat and have a relatively smaller effect on
227 the simulated strengthening of the PMOC. Over a longer time, the thermal density flux, which is
228 due to the loss of total heat, contributes more to the total density flux than the haline flux in relation
229 to reduction in the net freshwater discharge (Figure 6b). Spatially, both increased total density flux
230 and mixed layer depth in the North Pacific Ocean show opposite change characteristics with the
231 North Atlantic (Figure 7d). Correspondingly, in comparison to the MTP, there is a widespread
232 increase of the thermally induced density flux in the sub-polar North Pacific in NTP (Figure 7f), but
233 with little spatially changed in the haline density flux (Figure 7f). Thus, in contrast to the results
234 shown in the North Atlantic, the increased total heat exchange between the atmosphere and ocean
235 due to the processes of sensible and latent heat releases (Figure 6b) ultimately becomes a dominant
236 factor in maintaining a vigorous PMOC by controlling the increased total density flux (Figure 6a).

237 4. Conclusions and Discussion

238 This study investigates the effect of TP uplift on the large-scale oceanic circulation using a
239 low-resolution version of CESM. Results show that the removal of the TP initially changes the
240 wind-driven atmospheric moisture transport process and the wind-driven sea-ice coverage
241 expansion process, which are responsible for the initial weakening of the AMOC. Meanwhile, the
242 suppressed monsoonal circulation in East Asia and the western Pacific marginal seas induces the
243 decrease of rainfall and runoff and further causes the initially increased PMOC. Moreover, the
244 positive feedback further changes the AMOC and PMOC. In particular, the AMOC weakening can
245 further decrease the North Atlantic sea surface temperatures, ocean–atmosphere temperature
246 contrast, evaporation, and precipitation, and subsequently increase sea-ice coverage. These
247 processes together cause the final changes of the AMOC and PMOC (Figure 8).

248 A previous study demonstrated the role of Rocky Mountain uplift on heat transport and Gulf
249 Stream patterns in the North Atlantic (Seager et al., 2002). In this study, we focus on the most
250 prominent long-term orogenesis occurring since the Eocene: the TP and Himalayan uplift and
251 associated impacts on the MOC. Our results can be compared with those derived from the earlier
252 simulations, although experimental configurations differ somewhat. It has been indicated that the
253 removal of global mountains triggers the collapse of deep water in the North Atlantic but enables
254 formation in the North Pacific in three different coupled models (Schmittner et al., 2011; Sinha et
255 al., 2012; Maffre et al., 2017). The simulated weakening of the AMOC is also qualitatively
256 consistent with recent experiments using a decreased elevation of the TP and Central Asia (Fallah et
257 al., 2016). However, only TP topography is reduced in our study, but our results are comparable
258 with those of the ~~earlier~~past studies, therefore highlighting the key role that TP has played in
259 forming the current large-scale deep oceanic circulation pattern. Nevertheless, given that all existing
260 simulations (including ours) have used a rather coarse resolution of the coupled model
261 configuration, it is considered that a finer resolution model may provide a better representation of
262 the western boundary currents and allow for a more accurate and realistic resolving of the ocean
263 eddies, which are believed to be critically important oceanic processes that should be taken in the
264 realistic simulations of the AMOC (Spence et al., 2008). In addition, the low-resolution CESM is
265 also found to generally have a cold bias with the underestimated ocean heat transport and excessive
266 Arctic sea-ice (Shields et al., 2012), which could potentially exert modulations on the AMOC
267 weakening. It is thus considered that investigating the response of the PMOC and AMOC to the TP
268 uplift using an atmosphere–ocean general circulation model with a higher spatial resolution would
269 be useful. Besides, the robust changes in the AMOC and PMOC, and the associated mechanisms
270 due to the TP uplift can be evaluated through multi-model comparison.

271 Based on a comprehensive analysis of modern climatological data, Warren (1983) and
272 Emile-Geay et al. (2003) hypothesized that the present MOC (mainly occurring in the Atlantic but
273 not in the Pacific) is determined by the large mountains, namely the Himalayas and Rockies, which

274 induce an asymmetric distribution of wind stress and moisture transport features between the
275 Atlantic and Pacific basins. However, previous studies have also demonstrated that the asymmetric
276 continental extents and basin widths (basin geometries) between the two basins (Weaver et al., 1999;
277 Nilsson et al., 2013) also play a possible key role in maintaining the present day AMOC. Our
278 simulations support the hypothesis proposed by Warren (1983) and highlight the significant role of
279 the TP alone in maintaining the modern AMOC. Moreover, the similar PMOC–AMOC seesaw
280 dynamics have also been seen in simulations (Saenko et al., 2004; Chikamoto et al., 2012; Hu et al.,
281 2012) as well as in reconstructions (Okazaki et al., 2010; Menviel et al., 2014; Freeman et al., 2015)
282 for the last deglaciation. Such studies have also suggested that large PMOC–AMOC seesaw
283 modulations can be triggered by slight changes in the freshwater/salinity redistributions between the
284 Pacific and Atlantic. Furthermore, we provide an insight that the maintenance mechanism of PMOC
285 in [the simulation](#) without the TP, to some extent, is the same as the AMOC in the present day.
286 Specially, for the current North Atlantic, there is a persistently northward movement of warm and
287 salty water mass from the tropical-subtropical Gulf Stream region into North Atlantic and farther
288 poleward into the Norwegian and Greenland Seas, where it is exposed to very cold atmospheric
289 temperatures and followed by a gradual cooling and in turn a higher density due to the release
290 substantial sensible and latent heat into the overlying cold atmosphere, which is the same as PMOC,
291 before eventually forming the North Atlantic Deep Water.

292 Our simulations have potential implications for understanding paleotemperature reconstructions
293 and paleoceanographic circulation reorganization. The Earth has experienced a long-term cooling
294 trend throughout the Cenozoic as testified by many proxies and stacked records (Zachos et al., 2001,
295 2008), in association with an increased equator-to-pole thermal gradient. A very important
296 contribution to understanding the large cooling during the Cenozoic has been determined as the
297 drastic decrease in atmospheric CO₂ since the Eocene (DeConto and Pollard, 2003; DeConto et al.,
298 2008). On the other hand, a study with new data base further indicated that this thermal evolution
299 has been different among ocean basins during the Cenozoic (Cramer et al., 2009), and this differing

300 evolutionary pattern between basins is largely related to the large-scale ocean dynamics and tectonic
301 events (Zhang et al., 2011). Moreover, epsilon-Neodymium (eps-Nd) isotopes in the deep Pacific
302 suggest that the North Pacific was characterized by vigorous deep water formation during ca. 65–40
303 Ma (Thomas, 2004). Other new eps-Nd records also confirm that the overturning circulation was
304 already established in the high-latitude North Pacific prior to 40 Ma (Hague et al., 2012; Thomas et
305 al., 2014). ~~Comparatively~~In comparison, a modern-like bipolar oceanic circulation, characterized by
306 two branches of deep water formation in the Southern Ocean and the North Atlantic, began in the
307 late Eocene (~38.5 Ma) in relation to the effect of Southern Ocean gateway openings (Borrelli et al.,
308 2014). Several records also support that the onset of the present AMOC state began at the
309 Eocene–Oligocene transition (~34 Ma) in association with the tectonic deepening of the
310 Greenland–Norwegian Sea (Wright and Miller, 1993; Davies et al., 2001; Via and Thomas, 2006).
311 However, it is likely that the intermittent Cenozoic uplift of the TP reached a certain height by the
312 Early Oligocene, as shown in geologic evidences (Dupont-Nivet et al., 2008; Wang et al., 2008).
313 Our own contribution demonstrates that the major uplift occurring during this period was also an
314 important player in climate changes via hydrologic and ocean dynamics changes. Indeed, we
315 pinpoint the drastic effect of TP uplift alone on the distribution of the northern hemispheric MOCs
316 and potentially provide clues for proxy record interpretation.

317 Finally, this simulation is performed with the constant atmospheric CO₂ concentrations at the
318 pre-industrial, whereas it was higher during the uplift phase in the real world. In the context of past
319 warm world, such as Late Eocene, the climate conditions are accompanied by high atmospheric
320 CO₂ concentration, limited sea ice extent, and significantly modified land–sea distribution. Under
321 these warmer boundary conditions, the responses of AMOC to the TP induced freshwater forcing
322 may be very different from the modern conditions (e.g., Vavrus and Kutzbach, 2002). Therefore, it
323 will be necessary to perform further numerical experiments with more realistic boundary conditions
324 to accurately investigate the contribution of the TP uplift on the oceanic circulation and therefore to
325 be able to compare with data reconstructions.

326 *Acknowledgements* We sincerely thank the two anonymous reviewers for their insightful
327 comments and suggestions to improve this manuscript. We also thank Dr. Jiang Zhu for discussions
328 and technical support during the writing of the paper. This work was supported by the National
329 Natural Science Foundation of China (41421004, 41572159, and 41625018).

330 Reference

- 331 Abe, M., Kitoh, A., and Yasunari, T.: An evolution of the Asian summer monsoon associated with mountain
332 uplift—simulation with the MRI atmosphere-ocean coupled GCM, *J. Meteorol. Soc. Jpn.*, 81, 909–933,
333 2003.
- 334 An, Z., Kutzbach, J. E., Prell, W. L., and Porter, S. C.: Evolution of Asian monsoons and phased uplift of the
335 Himalaya–Tibetan plateau since Late Miocene times, *Nature*, 411, 62–66, 2001.
- 336 Bolin, B.: On the influence of the earth's orography on the general character of the westerlies, *Tellus*, 2, 184–195,
337 1950.
- 338 Borrelli, C., Cramer, B. S., and Katz, M. E.: Bipolar Atlantic deepwater circulation in the middle-late Eocene:
339 Effects of southern ocean gateway openings, *Paleoceanography*, 29, 308–327, 2014.
- 340 Botsyun, S., Sepulchre, P., Risi, C., Donnadieu, Y.: Impacts of Tibetan Plateau uplift on atmospheric dynamics and
341 associated precipitation $\delta^{18}\text{O}$, *Clim. Past*, 12, 1401–1420, 2016.
- 342 Broccoli, A. J., and Manabe, S.: The effects of orography on midlatitude northern hemisphere dry climates, *J.*
343 *Clim.*, 5, 1181–1201, 1992.
- 344 Chikamoto, M. O., Menviel, L., Abe-Ouchi, A., Ohgaito, R., Timmermann, A., Okazaki, Y., Harada, N., Oka, A.,
345 and Mouchet, A.: Variability in North Pacific intermediate and deep water ventilation during Heinrich
346 events in two coupled climate models, *Deep-Sea Res. PT. II*, 61–64, 114–126, 2012.
- 347 Cramer, B. S., Toggweiler, J. R., Wright, J. D., Katz, M. E., and Miller, K. G.: Ocean overturning since the Late
348 Cretaceous: Inferences from a new benthic foraminiferal isotope compilation, *Paleoceanography*, 24,
349 PA4216, doi:10.1029/2008PA001683, 2009.
- 350 Cunningham, S. A., Kanzow, T., Rayner, D., Baringer, M. O., Johns, W. E., Marotzke, J., Longworth, H. R., Grant,
351 E. M., Hirschi, J. J.-M., Beal, L. M., Meinen, C. S., and Bryden, H. L.: Temporal variability of the Atlantic
352 meridional overturning circulation at 26.5°N, *Science*, 317, 935–938, doi:10.1126/science.1141304, 2007.
- 353 Davies, R., Cartwright, J., Pike, J., and Line, C.: Early Oligocene initiation of North Atlantic deep water formation,
354 *Nature*, 410, 917–920, 2001.
- 355 DeConto, R. M., and Pollard, D.: Rapid Cenozoic glaciation of Antarctica induced by declining atmospheric CO₂,
356 *Nature*, 421, 245–249, 2003.
- 357 DeConto, R. M., Pollard, D., Wilson, P. A., Pälike, H., Lear, C., and Pagani, M.: Thresholds for Cenozoic bipolar
358 glaciation, *Nature*, 455, 652–657, 2008.
- 359 Dupont-Nivet, G., Hoorn, C., and Konert, M.: Tibetan uplift prior to the Eocene-Oligocene climate transition:
360 Evidence from pollen analysis of the Xining Basin, *Geology*, 36, 987–990, 2008.
- 361 Emile-Geay, J., Cane, M. A., Naik, N., Seager, R., Clement, A. C., and van Geen, A.: Warren revisited:
362 Atmospheric freshwater fluxes and “Why is no deep water formed in the North Pacific”, *J. Geophys. Res.*,
363 108(C6), 3178, doi:10.1029/2001JC001058, 2003.

364 Fallah, B., Cubasch, U., Prömmel, K., and Sodoudi, S.: A numerical model study on the behaviour of Asian
365 summer monsoon and AMOC due to orographic forcing of Tibetan Plateau, *Clim. Dyn.*, 47, 1485–1495,
366 2016.

367 Feng, R., and Poulsen, C. J.: Andean elevation control on tropical Pacific climate and ENSO, *Paleoceanography*,
368 29, 795–809, 2014.

369 Freeman, E., Skinner, L. C., Tisserand, A., Dokken, T., Timmermann, A., Menviel, L., and Friedrich, T.: An
370 Atlantic–Pacific ventilation seesaw across the last deglaciation, *Earth Planet. Sci. Lett.*, 424, 237–244,
371 2015.

372 Gent, P. R., Danabasoglu, G., Donner, L. J., Holland, M. M., Hunke, E. C., Jayne, S. R., Lawrence, D. M., Neale,
373 R. B., Rasch, P. J., Vertenstein, M., Worley, P. H., Yang, Z. L., and Zhang, M.: The Community Climate
374 System Model version 4, *J. Clim.*, 24, 4973–4991, doi:10.1175/2011JCLI4083.1, 2011.

375 Hague, A. M., Thomas, D. J., Huber, M., Korty, R., Woodard, S. C., and Jones, B. L.: Convection of North Pacific
376 deep water during the early Cenozoic, *Geology*, 40, 527–530, 2012.

377 Holland, M. M., Bailey, D. A., Briegleb, B. P., Light, B., and Hunke, E.: Improved sea ice shortwave radiation
378 physics in CCSM4: The impact of melt ponds and black carbon, *J. Clim.*, 25, 1413–1430, 2012.

379 Hu, A., Meehl, G. A., Han, W., Timmermann, A., Otto-Bliesner, B., Liu, Z., Washington, W. M., Large, W.,
380 Abe-Ouchi, A., Kimoto, M.: Role of the Bering Strait on the hysteresis of the ocean conveyor belt
381 circulation and glacial climate stability, *Proc. Natl. Acad. Sci. U. S. A.*, 109, 6417–6422, 2012.

382 Jayne, S. R., and Marotzke, J.: A destabilizing thermohaline circulation–atmosphere–sea ice feedback, *J. Clim.*, 12,
383 642–651, 1999.

384 Jiang, D., Ding, Z. L., Drange, H., and Gao, Y.: Sensitivity of East Asian climate to the progressive uplift and
385 expansion of the Tibetan Plateau under the mid-Pliocene boundary conditions, *Adv. Atmos. Sci.*, 25,
386 709–722, 2008.

387 Kitoh, A.: Effects of mountain uplift on East Asian summer climate investigated by a coupled atmosphere–ocean
388 GCM, *J. Clim.*, 17, 783–802, 2004.

389 Kutzbach, J. E., Prell, W. L., and Ruddiman, W. F.: Sensitivity of Eurasian climate to surface uplift of the Tibetan
390 Plateau, *J. Geol.*, 101, 177–190, 1993.

391 Liu, X., and Yin, Z.-Y.: Sensitivity of East Asian monsoon climate to the uplift of the Tibetan Plateau, *Palaeogeogr.*
392 *Palaeoclim. Palaeoecol.*, 183, 223–245, 2002.

393 Maffre, P., Ladant, J. B., Donnadieu, Y., Sepulchre, P., and Godd eris, Y.: The influence of orography on modern
394 ocean circulation, *Clim. Dyn.*, doi:10.1007/s00382-017-3683-0, 2017.

395 Menviel, L., England, M. H., Meissner, K. J., Mouchet, A., and Yu, J.: Atlantic-Pacific seesaw and its role in
396 outgassing CO₂ during Heinrich events, *Paleoceanography*, 29, 58–70, 2014.

397 Molnar, P., Boos, W. R., and Battisti, D. S.: Orographic controls on climate and paleoclimate of Asia: Thermal and
398 mechanical roles for the Tibetan Plateau, *Annu. Rev. Earth. Planet. Sci.*, 38, 77–102, 2010.

399 Nilsson, J., Langen, P., Ferreira, D., and Marshall, J.: Ocean basin geometry and the salinification of the Atlantic
400 Ocean, *J. Clim.*, 26, 6163–6184, 2013.

401 Okajima, H., and Xie, S. P.: Orographic effects on the northwestern Pacific monsoon: Role of air-sea interaction,
402 *Geophys. Res. Lett.*, 34, L21708, doi: 10.1029/2007GL032206, 2007.

403 Okazaki, Y., Timmermann, A., Menviel, L., Harada, N., Abe-Ouchi, A., Chikamoto, M. O., Mouchet, A., and
404 Asahi, H.: Deepwater formation in the North Pacific during the last glacial termination, *Science*, 329,
405 200–204, 2010.

406 Palmer, T. N., Shutts, G. J., and Swinbank, R.: Alleviation of a systematic westerly bias in general circulation and
407 numerical weather prediction models through an orographic gravity wave drag parametrization, *Q. J. R.
408 Meteorol. Soc.*, 112, 1001–1039, 1986.

409 Ramstein, G., Fluteau, F., Besse, J., and Joussaume, S.: Effect of orogeny, plate motion and land-sea distribution
410 on Eurasian climate change over the past 30 million years, *Nature*, 386, 788–795, 1997.

411 Rind, D., Russell, G., and Ruddiman, W. F.: The effects of uplift on Ocean–Atmosphere, in: *Tectonic Uplift and
412 Climate Change*, Ruddiman, W. F. (Ed.), Plenum Press, New York, 123–147, 1997.

413 Rodwell, M. J., and Hoskins, B. J.: Subtropical anticyclones and summer monsoons, *J. Clim.*, 14, 3192–3211,
414 2001.

415 Ruddiman, W. F., and Kutzbach, J. E.: Forcing of Late Cenozoic northern hemisphere climate by plateau uplift in
416 southern Asia and the American West, *J. Geophys. Res.*, 94(D15), 18409–18427, 1989.

417 Saenko, O. A., Schmittner, A., and Weaver, A. J.: The Atlantic-Pacific seesaw, *J. Clim.*, 17, 2033–2038, 2004.

418 Schmitt, R. W., Bogden, P. S., and Dorman, C. E.: Evaporation minus precipitation and density fluxes for the
419 North Atlantic, *J. Phys. Oceanogr.*, 19, 1208–1221, 1989.

420 Schmittner, A., Silva, T. A. M., Fraedrich, K., Kirk, E., and Lunkeit, F.: Effects of mountains and ice sheets on
421 global ocean circulation, *J. Clim.*, 24, 2814–2829, 2011.

422 Seager, R., Battisti, D. S., Yin, J., Gordon, N., Naik, N., Clement, A. C., and Cane, M. A.: Is the Gulf Stream
423 responsible for Europe's mild winters?, *Q. J. R. Meteorol. Soc.*, 128, 2563–2586, 2002.

424 Sepulchre, P., Sloan, L. C., Snyder, M., and Fiechter, J.: Impacts of Andean uplift on the Humboldt Current system:
425 A climate model sensitivity study, *Paleoceanography*, 24, PA4215, doi:10.1029/2008PA001668, 2009.

426 Shields, C. A., Bailey, D. A., Danabasoglu, G., Jochum, M., Kiehl, J. T., Levis, S., and Park, S.: The
427 low-resolution CCSM4, *J. Clim.*, 25, 3993–4014, 2012.

428 Sinha, B., Blaker, A. T., Hirschi, J., Bonham, S., Brand, M., Josey, S., Smith, R. S., and Marotzke, J.: Mountain
429 ranges favour vigorous Atlantic meridional overturning, *Geophys. Res. Lett.*, 39, L02705,
430 doi:10.1029/2011GL050485, 2012.

431 Spence, J., Eby, M., and Weaver, A.: The sensitivity of the Atlantic meridional overturning circulation to
432 freshwater forcing at eddy-permitting resolutions, *J. Clim.*, 21, 2697–2710, 2008.

433 Thomas, D. J.: Evidence for deep-water production in the North Pacific Ocean during the early Cenozoic warm
434 interval, *Nature*, 430, 65–68, 2004.

435 Thomas, D. J., Korty, R., Huber, M., Schubert, J. A., and Haines, B.: Nd isotopic structure of the Pacific Ocean
436 70–30 Ma and numerical evidence for vigorous ocean circulation and ocean heat transport in a greenhouse
437 world, *Paleoceanography*, 29, 454–469, 2014.

438 Vavrus, S., and Kutzbach, J. E.: Sensitivity of the thermohaline circulation to increased CO₂ and lowered
439 topography, *Geophys. Res. Lett.*, 29, 1546, doi:10.1029/2002GL014814, 2002.

440 Via, R. K., and Thomas, D. J.: Evolution of Atlantic thermohaline circulation: Early Oligocene onset of
441 deep-water production in the North Atlantic, *Geology*, 34, 441–444, 2006.

442 Wang, C., Zhao, X., Liu, Z., Lippert, P. C., Graham, S. A., Coe, R. S., Yi, H., Zhu, L., Liu, S., and Li, Y.:
443 Constraints on the early uplift history of the Tibetan Plateau, *Proc. Natl. Acad. Sci. U. S. A.*, 105,
444 4987–4992, 2008.

445 Warren, B. A.: Why is no deep water formed in the North Pacific?, *J. Mar. Res.*, 41, 327–347, 1983.

446 Weaver, A. J., Bitz, C. M., Fanning, A. F., and Holland, M. M.: Thermohaline circulation: High-latitude
447 phenomena and the difference between the Pacific and Atlantic, *Annu. Rev. Earth. Planet. Sci.*, 27, 231–285,
448 1999.

449 Wright, J. D., and Miller, K. G.: Southern ocean influences on late Eocene to Miocene deepwater circulation, in:
450 The Antarctic Paleoenvironment: A perspective on global change part two, Kennett, J. P. and Warnke, D. A.
451 (Eds.), American Geophysical Union, Washington, 1–25, 1993.

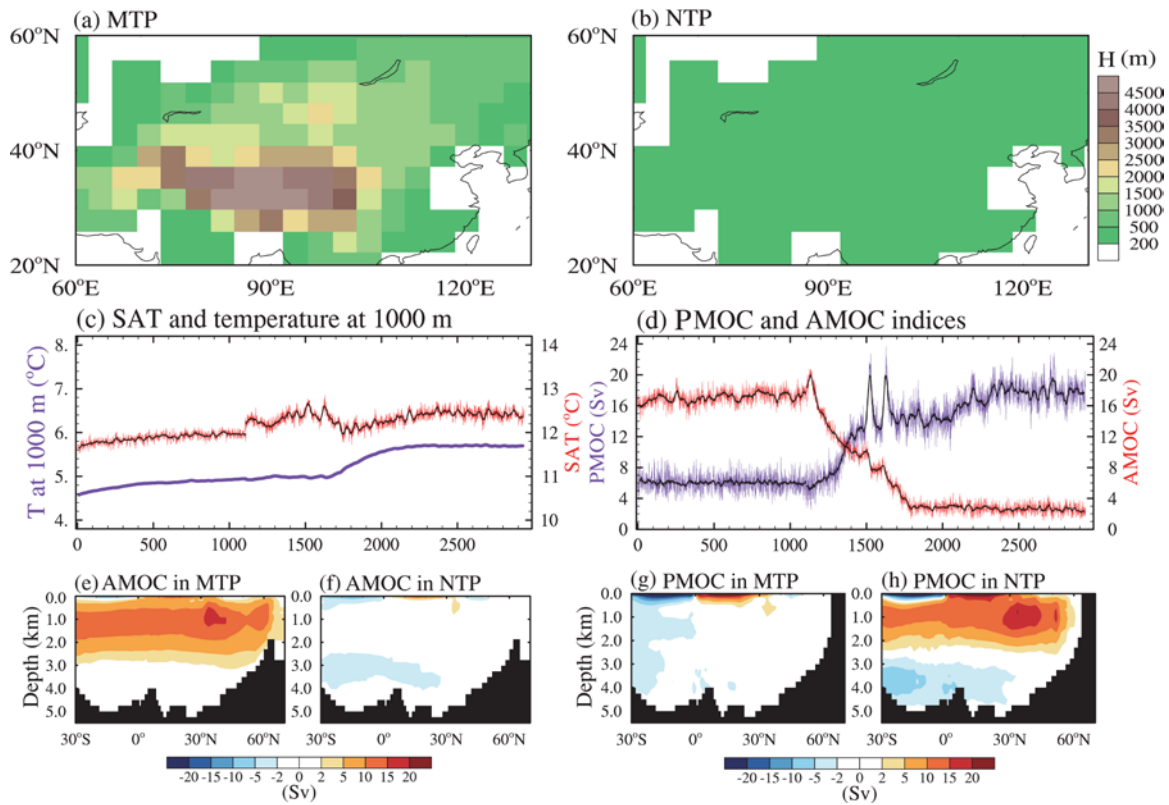
452 Zachos, J., Pagani, M., Sloan, L., Thomas, E., and Billups, K.: Trends, rhythms, and aberrations in global climate
453 65 Ma to present, *Science*, 292, 686–693, 2001.

454 Zachos, J. C., Dickens, G. R., and Zeebe, R. E.: An early Cenozoic perspective on greenhouse warming and
455 carbon-cycle dynamics, *Nature*, 451, 279–283, 2008.

456 Zhang, R., Jiang, D., Zhang, Z., and Yu, E.: The impact of regional uplift of the Tibetan Plateau on the Asian
457 monsoon climate, *Palaeogeogr. Palaeoclim. Palaeoecol.*, 417, 137–150, 2015.

458 Zhang, Z., Nisancioglu, K. H., Flatoy, F., Bentesen, M., Bethke, I., and Wang, H.: Tropical seaways played a more
459 important role than high latitude seaways in Cenozoic cooling, *Clim. Past*, 7, 801–813, 2011.

460 Zhu, J., Liu, Z., Zhang, X., Eisenman, I., and Liu, W.: Linear weakening of the AMOC in response to receding
461 glacial ice sheets in CCSM3, *Geophys. Res. Lett.*, 41, 6252–6258, 2014.



462

463 **Figure 1.** Two topographic height configurations used in experiments: (a) MTP and (b) NTP. (c)

464 Time series of global mean annual 2-m surface air temperature (SAT) and sea temperature at 1000

465 m depth in MTP (1–1100 years) and NTP (1101–2940 years) simulations; bold black lines show

466 21-year running mean. (d) Same as (c) but for PMOC and AMOC indices, respectively. AMOC and

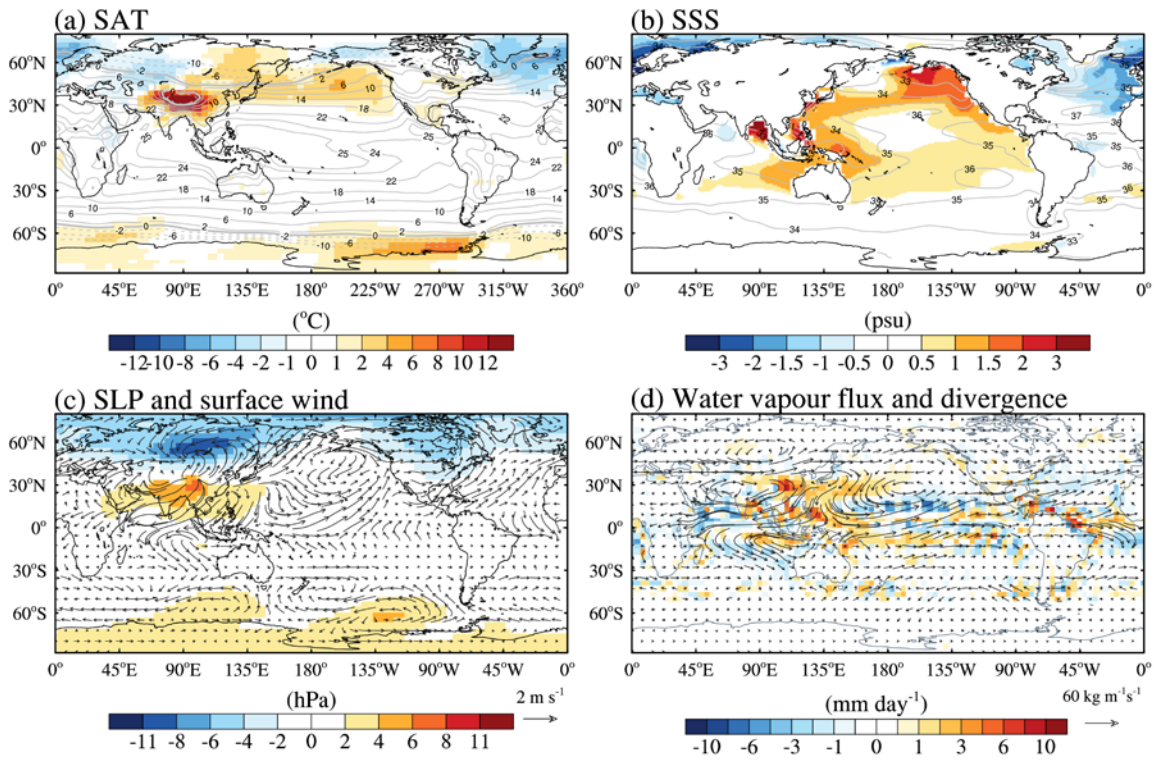
467 PMOC indices are defined as the annual maximum of the meridional stream function value north of

468 28°N and below the depth of 500 m over the North Atlantic and Pacific, respectively. (e–h)

469 Climatological annual mean Atlantic and Indian–Pacific meridional overturning stream function in

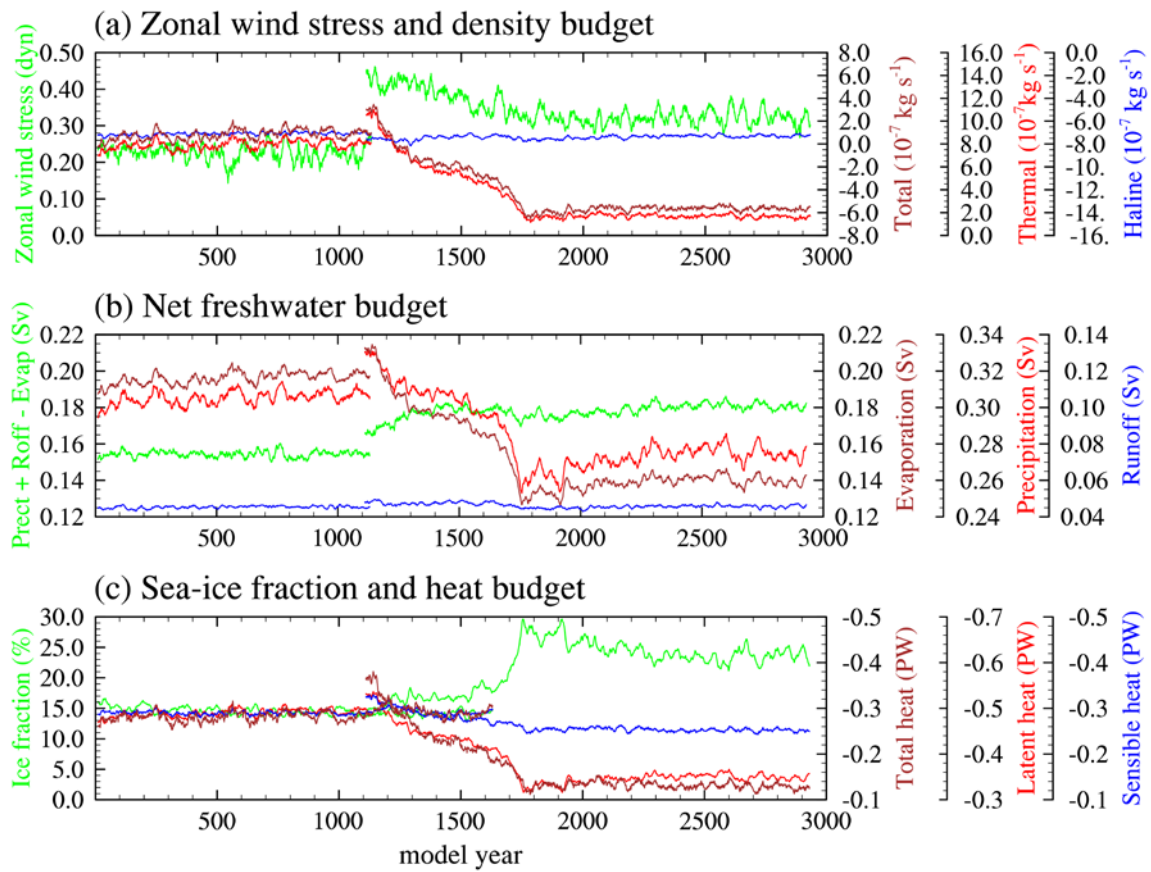
470 MTP (e and g) and NTP (f and h); positive (negative) shading represents clockwise

471 (counterclockwise) circulations.



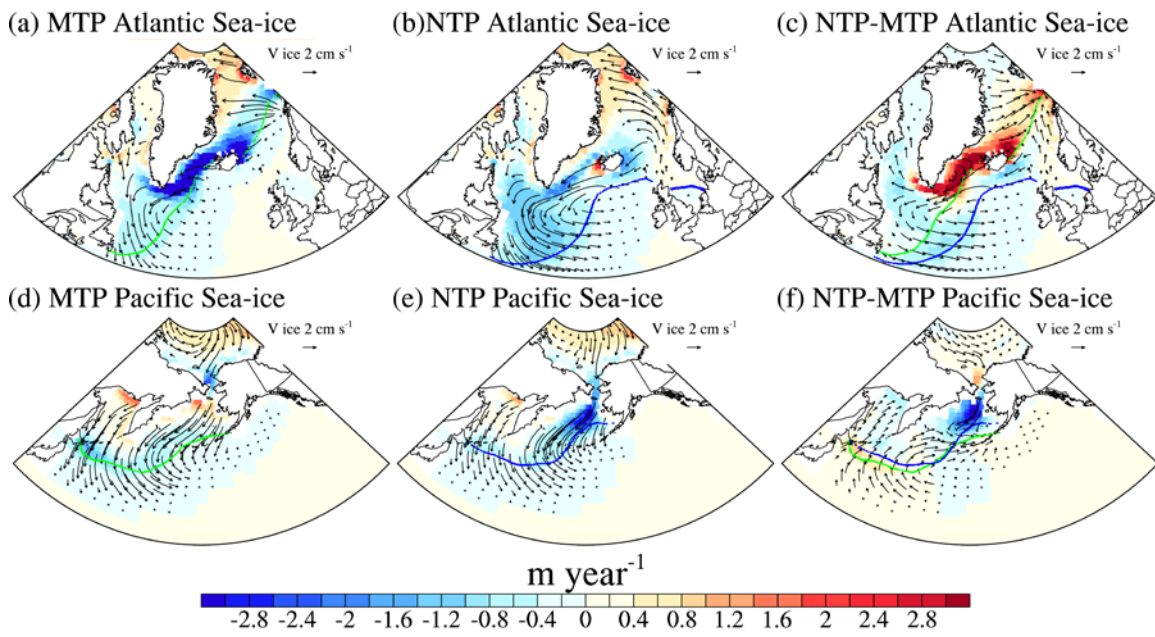
472

473 **Figure 2.** (a) Climatological SAT in MTP (contour) and anomalies (shaded) for NTP minus MTP;
 474 (b) same as Figure 2a, but for sea surface salinity (SSS); (c) changes in sea-level pressure (SLP,
 475 shading) and surface wind (vectors); and (d) vertically integrated (surface to 300 hPa pressure layer)
 476 water vapor flux (vectors) and its convergence (shading) in NTP relative to MTP. Unit of
 477 convergence is converted to mm day^{-1} assuming the density of liquid water as 1 g cm^{-3} .



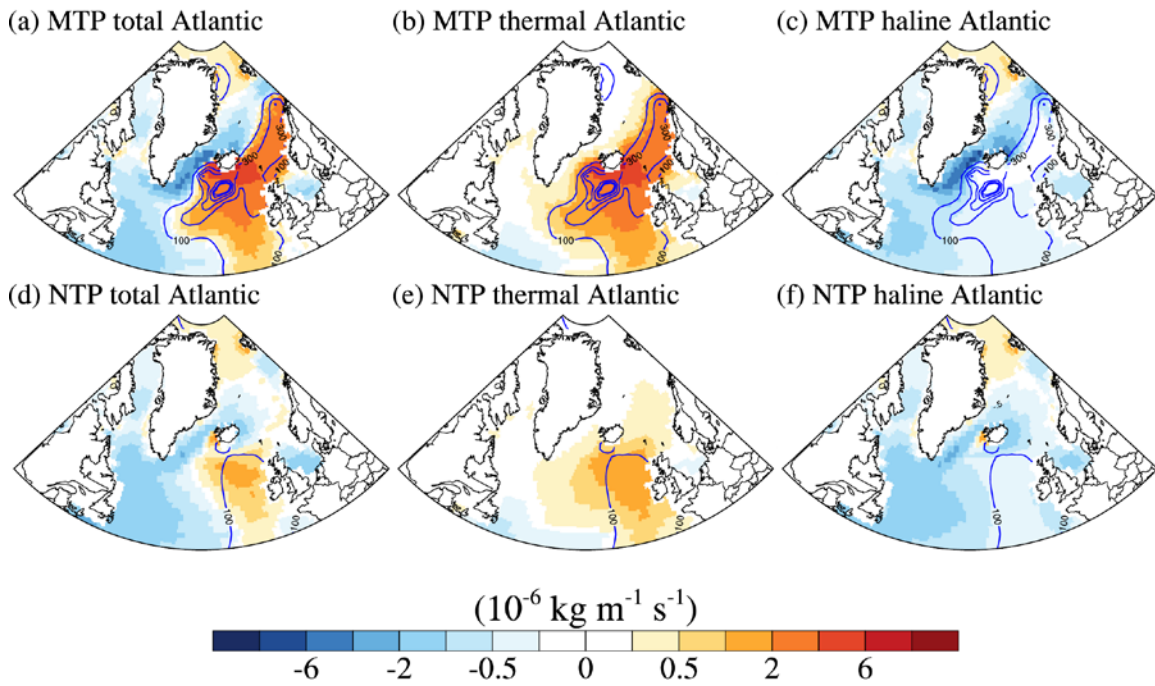
478

479 **Figure 3.** Regional annual mean across North Atlantic basin at 40° – 70° N for MTP (1–1100 years)
 480 and NTP (1101–2940 years) of (a) zonal surface wind-stress, total density flux, haline density flux,
 481 and thermal density flux (total density flux is decomposed into haline contribution due to freshwater
 482 flux and thermal contribution due to heat flux (*Schmitt et al.*, 1989); (b) net freshwater, precipitation,
 483 runoff, and evaporation fluxes; (c) sea-ice fraction, total heat, sensible heat, and latent heat fluxes,
 484 (units: PW, $1 \text{ PW} = 10^{15} \text{ W}$). For comparison purposes, all lines with common units use identical
 485 vertical scale spacing.



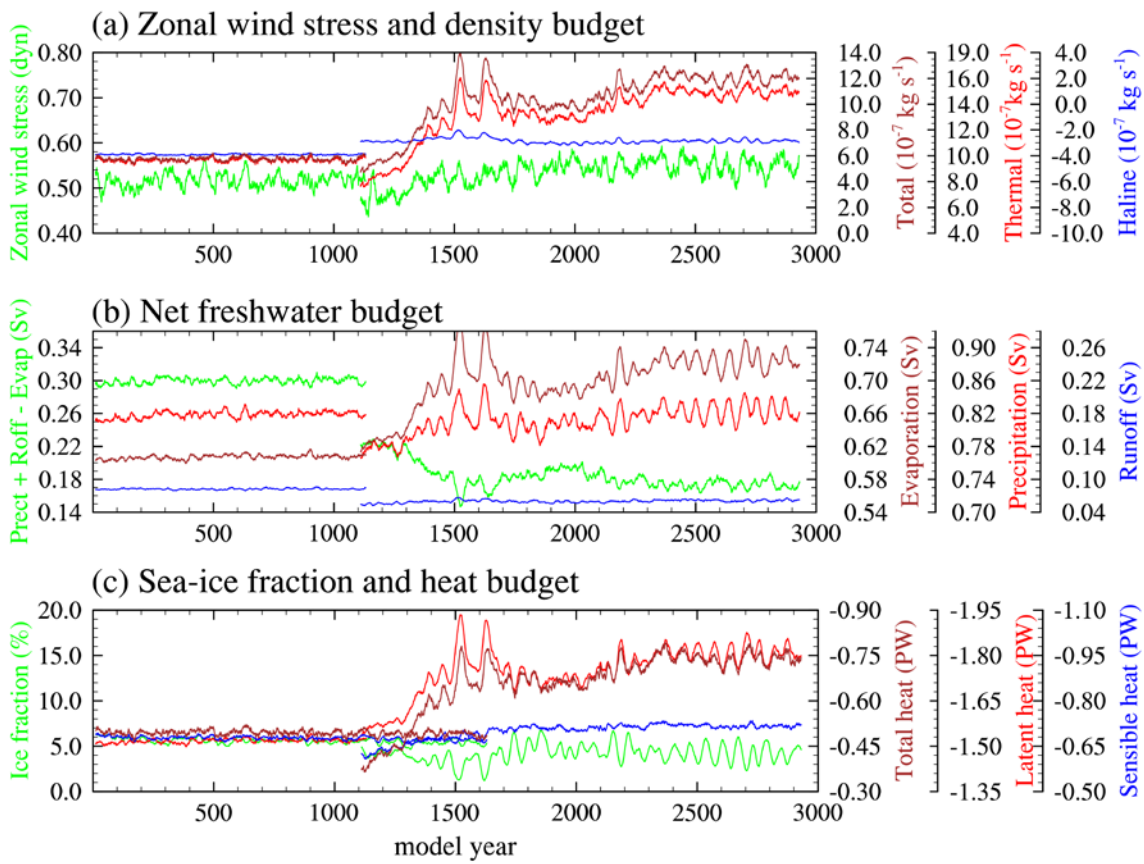
486

487 **Figure 4.** The North Atlantic and Pacific region features of annual mean sea-ice formation rate
 488 (shading; positive stands for formation, and negative stands for melting), sea-ice velocity (vectors,
 489 cm s^{-1}), and for (a, d) MTP, (b, e) NTP, and (c, f) difference between NTP and MTP. The February
 490 sea-ice margin is indicated with dashed lines (defined as the 15% sea-ice coverage, green line for
 491 MTP, blue line for NTP)



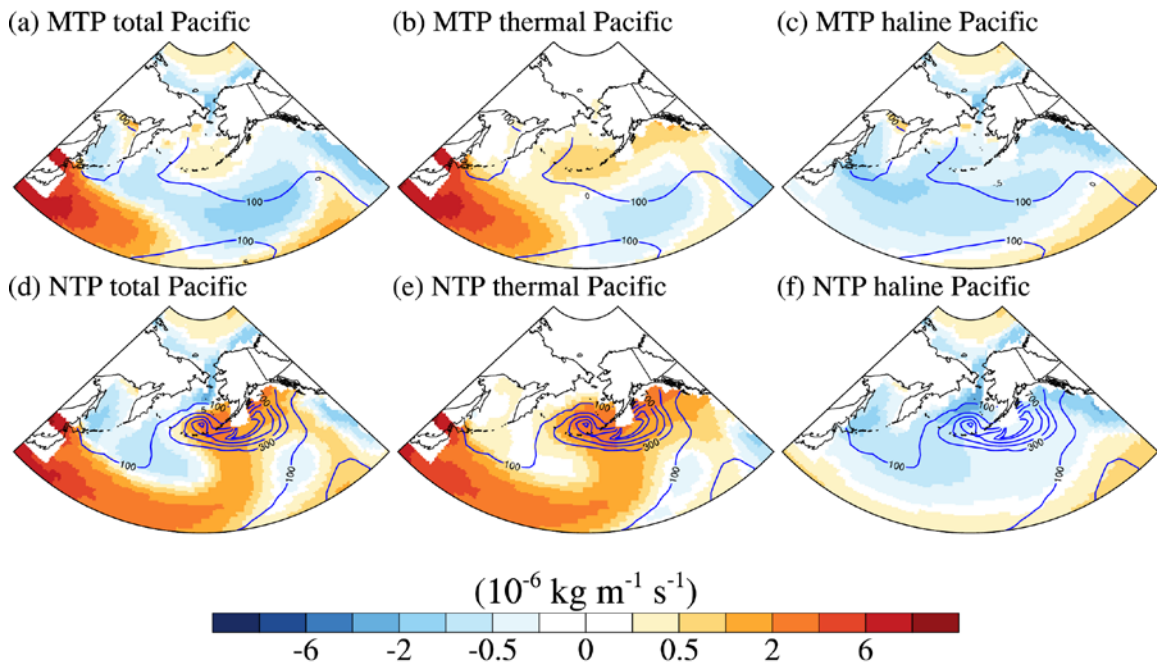
492

493 **Figure 5.** The North Atlantic annual mean (a, d) total density flux (shading; positive means flux
 494 makes water denser), (b, e) the thermal density flux, (c, f) the haline density flux, and the winter
 495 mixed layer depth (blue contour, contour interval: 200 m) in the MTP (upper panel) and NTP (lower
 496 panel).



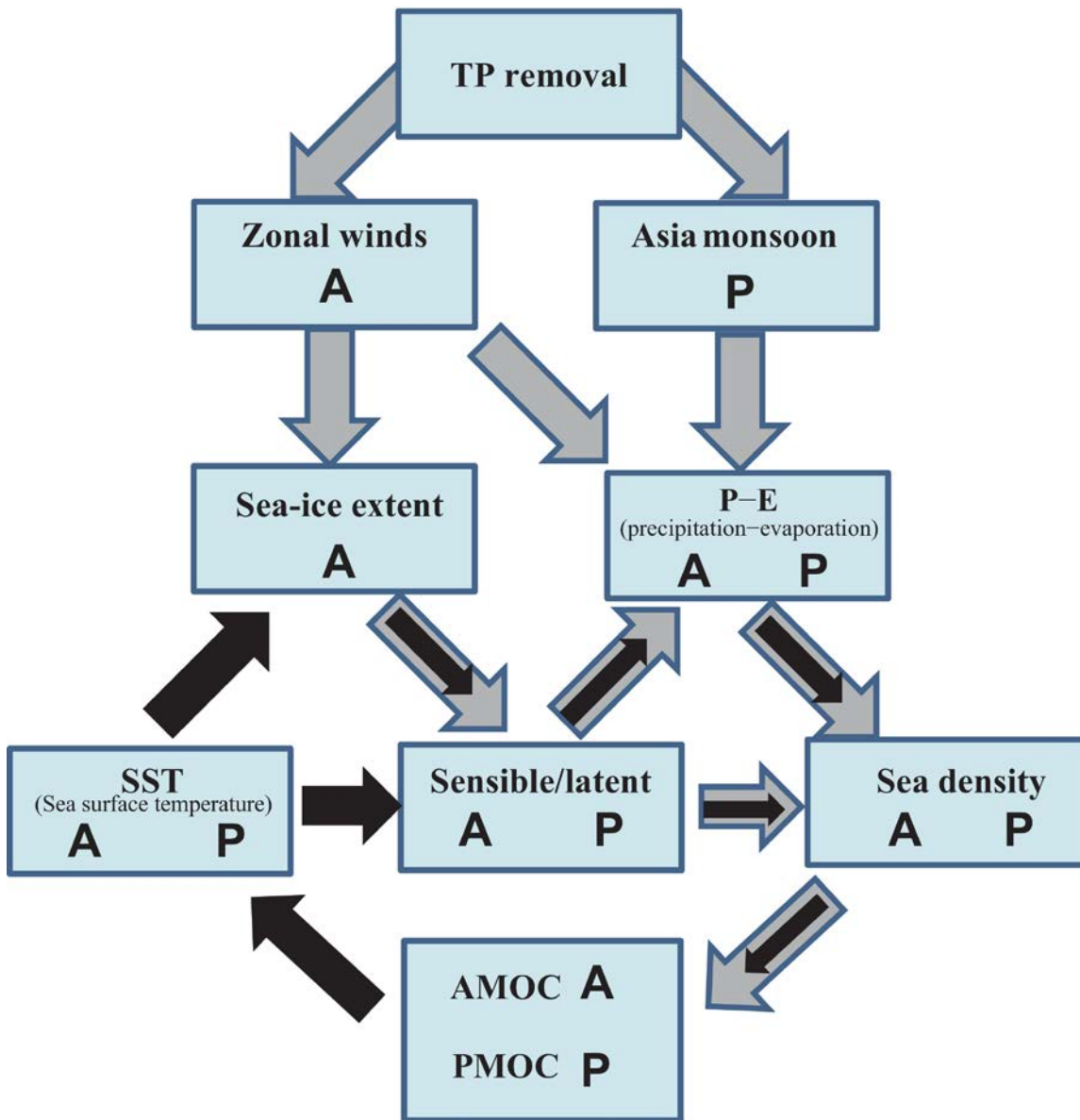
497

498 **Figure 6.** As in Figure 3, but for North Pacific basin at 30°–70°N.



499

500 **Figure 7.** The same as Figure 5, but for the North Pacific (30–80°N).



501

502 **Figure 8.** Schematic diagram about the influence of the removal of TP on the AMOC and PMOC.

503 Vectors in gray denote the climate responses in relation to the increased in wind-induced and
 504 decreased monsoonal-driven net precipitation-evaporation and wind-driven sea-ice processes. The

505 black color vectors denote the feedback processes. The bold characters A and P stand for the

506 physical processes occurring over the North Atlantic and Pacific, respectively.